Magnetically tunable damping in composites for 4D printing

Federico Guillermo Bonifacich [1], Osvaldo Agustín Lambri [1], Vicente Recarte [2,3,*], Vicente Sánchez-Alarcos [2,3], José Ignacio Pérez-Landazábal [2,3]

[1] CONICET-UNR. Laboratorio de Materiales, Escuela de Ingeniería Eléctrica, Centro de Tecnología e Investigación Eléctrica (CETIE), Facultad de Ciencias Exactas, Ingeniería y Agrimensura, Avda. Pellegrini 250, (2000) Rosario, Argentina

[2] Departamento de Ciencias, Universidad Pública de Navarra, Campus de Arrosadía, 31006 Pamplona, Spain

[3] Institute for Advanced Materials and Mathematics (INAMAT^2), Universidad Pública de Navarra, Campus de Arrosadía, 31006 Pamplona, Spain

*Corresponding Author:

Vicente Recarte

e-mail address: recarte@unavarra.es

Abstract

Composite materials are being used in the design of new devices to produce more functional, cheap and on-demand products. In particular, 3D printing technology based on composites opens a huge field enabling the freedom of design and the ability to manufacture complex structures. In this context, the analysis of the functional properties of printable composites is of great importance. The work is focused on the analysis of the mechanical damping of a composite made with different concentrations of a $Ni_{45}Mn_{36.7}In_{13.3}Co_5$ metamagnetic shape memory alloy into an UV-curing polymer. The composites provide a bulk material containing very brittle metallic μ-particles that can be handled for technological applications. Damping and dynamic modulus of the composites were modified with small magnetic fields below 100kA/m, proving that the damping capacity can be tuned by applying an external magnetic field. From the measurements, it has been also possible to determine the intrinsic damping and moduli of the alloy particles, which show the characteristic properties linked to the MT. These preliminary results allow proposing this composite material as a potential functional material to be used in the design of printable devices for magneto-mechanical damping applications.

Keywords

Multifunctional composites (A)

Polymer-matrix composites (PMCs) (A)

Shape memory behavior (B)

Thermomechanical properties (B)

Anelasticity (C)

1. *Introduction*

The vast interest and the widespread research effort dedicated to metamagnetic shape memory alloys (MSMAs) in the last decade stems from their potential as multifunctional materials, based on the interplay between a first-order structural transition – the martensitic transformation (MT) – and the magnetic ordering. In particular, the possibility of inducing the reverse MT by applying a magnetic field gives rise to interesting properties such as the magnetic actuation [1,2] or the giant inverse magnetocaloric effect (MCE) [3,4] that make these alloys very attractive for actuating and magnetic refrigeration applications. Besides, the inherent damping properties of shape memory alloys can be used for active noise reduction and mechanical damping applications [5,6], being able to control the damping by an external magnetic field through the hysteretic induced MT. In general, their intrinsic brittleness limits the applicability of MSMA, but for some specific applications, like damping or magnetic cooling devices, brittleness is not so critical and could be mitigated by making MSMA/polymer composites.

Three-dimensional (3D) printing is an additive manufacturing technology that allows fabrication of objects by adding successive layers of materials. In recent years, this technique has become very popular because of its simplicity, relatively low cost, and unlimited creativity. This process enables the creation of complex three-dimensional objects, which cannot be cut, assembled or carved otherwise. 3D printing has developed rapidly and has found numerous applications in various fields, from personalized consumer products, dentistry and surgery, biomaterials and tissue engineering, to different kind of materials for structural and sensor-actuators applications [7-13]. 3D printing composites materials which exhibit special tunable

(using an external magnetic field i.e.?) characteristics are referred to as 4D printed composites [13].

There are several 3D printing techniques based on mechanical, electrical, or photochemical approaches, each of them having its advantages and drawbacks [7,14-19]. The photochemical approach has been proved to be very promising since well-defined structures can be created by photopolymerization of photocrosslinkable liquid resin under light irradiation, being also an economic and low environmental impact technique [20,21].

Additive manufacturing of MSMA-polymer composites is cheaper and simpler than metal printing, allowing to build for example, a heat exchanger device with the optimum surface/volume ratio for MCE applications. Then, 3D printed MSMA/polymer composites are promising materials for damping and refrigeration applications. In fact, composites in sandwich geometry [22] and composites of Ni-Mn-Ga powders in a polymer matrix [22-27], have been investigated. In the Ni-Mn-In system, the addition of Co has been shown to increase the Curie temperature and the saturation magnetization in the austenite phase, as well and the blocking stress level, thus reducing the value of the applied magnetic field needed to induce the reverse MT [1,28]. Quaternary Ni-Mn-In-Co alloys are, therefore, the most promising alloys for functional composites elaboration.

In the present work, the damping properties of composites elaborated with different concentrations of Ni-Mn-In-Co particles into a printable polymer have been analyzed. The developed composites provide a bulk material, containing very brittle metallic particles as fillers, which can be handled for technological applications. The composites have a good mechanical stability and reflect the magnetic properties of the MSMA-fillers. In particular, the damping capacity can be tuned when the composites

are subjected to an external magnetic field. The fillers slightly shift the glass transition temperature of the polymer to higher temperature. Damping and dynamic modulus of the composites were modified with small magnetic fields below 100kA/m. The good mechanical properties and the possibility of modifying its response under the application of the magnetic field shown by the composites, open the possibility of using these materials for 3-D printing as the basis for devices for MCE and magnetomechanical damping.

2. *Experimental*

2.1. *Samples*

$Ni_{45}Mn_{36.7}In_{13.3}Co_5$ ingots were produced by arc-melting, under Argon atmosphere from pure metals. Ingots were homogenized at 1073 K for 24 hours under Argon atmosphere followed by quenching in air. Bulk sample was milled and sieved. Particles smaller than 63μm were used as fillers to prepare the composite. For relieving the stresses originated during the grinding, the powder was annealed at 423 K for 900 s, under protective Argon atmosphere.

The polymeric matrix was a commercial photo curable bisphenol A-glycidyl methacrylate (Bis-GMA) resin produced by Schmidt (Composite flow). The polymeric resin contains fillers of glass (28% vol., size 0.05-2.6 mm), catalyst, stabilizers, inhibitors and pigments in a concentration smaller than 53% vol.

The MSMA-particles and the polymer resin were well mixed by hand-stirring, to reach a homogeneous mixture. Different exposure times were considered to optimize the curing process using UV light (600 mW/cm^2, 410 nm) at room temperature (RT). The crosslinking evolution reaches the saturation value after an exposure of 80 s under the UV light. Composites with 1.1%, 2.6%, 6.2% and 12.8%, volume fractions of fillers

were prepared, referred to as C011, C026, C062 and C128, respectively (see Table 1). The fillers concentration was determined with a 50 ml pycnometer at 20°C using distilled water. In this stadium, the composites were not subjected to any 3D printing process. This paper is a first approach to determine the potential of the composites for mechanical damping applications based on a photo curable polymeric resin.

	Volume fraction (%)	**Density [g cm^{-3}]**	**Shear modulus at RT (MPa)**	**tan(ϕ) at RT**	**tan(ϕ) at Tg**
Matrix		1.85±0.01	500±10	0.164±0.002	0.345±0.004
C011	1.1±0.3	1.92±0.01	670±20	0.178±0.002	0.339±0.004
C026	2.6±0.5	2.01±0.02	840±20	0.195±0.002	0.333±0.004
C062	6.2±0.5	2.23±0.02	1490±40	0.193±0.002	0.323±0.003
C128	12.8±0.6	2.64±0.02	2620±70	0.196±0.002	0.321±0.003

Table 1: Volume fraction, density, dynamic shear modulus and tan(ϕ) at room temperature (RT) and tan(ϕ) at Tg for polymeric and composite samples.

2.2. *Measurements*

MagnetoThermoGravimetry (MTGA) studies were performed in a modified Radwag AS 220.R2 balance from 200 K up to 400 K under protective Argon atmosphere with a heating rate of 5K/minute and under an axial magnetic field of 100 kA/m. During the MTGA measurement, the weight (force) variation percentage ρ_M(T), which is proportional to the changes in the magnetization, is determined from:

$$\rho_M(\mathrm{T}) = \frac{w(\mathrm{T}) - w_i}{w_i} \qquad (1)$$

where w_i and $w(T)$ are the initial weight measured at 200 K and the weight measured at each temperature (T), respectively.

Dynamic Mechanical Analysis (DMA) measurements, loss tangent (damping or internal friction, Q^{-1}), tan(ϕ), and dynamic shear modulus, G', were carried out in an inverted torsion pendulum which was assembled at the laboratory. The excitation was controlled by a Rigol DG1022 sintetized wave function generator and the oscillations were recorded by a Rigol DS1052E high speed digital oscilloscope. Temperature of the sample was measured using a K-thermocouple close to the sample. The A/D conversion from the temperature signal was done by means of a Flüke 289 (true RMS multimeter). All the system is automatically driven by a PC during heating and cooling using a NOVUS-N2000 PID temperature controller. Measurements were performed as a function of temperature at frequencies close to 5 Hz. The samples for DMA were parallelepiped bars of around 1 x 1 x 20 mm^3. The maximum shear strain on the sample was $2x10^{-4}$. Measurements were performed during heating and cooling with a rate of 1K/min in a temperature range between 220 K and 400 K. A thermal cycle in DMA measurements involves a cooling down from RT to 220 K, followed by a warming up to 400 K and subsequently a cooling down to RT. There were not holding time neither at the minimum nor at the maximum temperatures. Two consecutive thermal cycles were performed for all studied samples under atmospheric Argon pressure. Nonetheless, for the sample with the highest particles content, ten thermal cycles were performed to explore the stability of the composite.

Damping was determined by measuring the relative half width of the squared resonance peak for a specimen driven into forced vibration using [29]:

$$\tan(\phi) = \frac{\omega_2 - \omega_1}{\omega_0} \qquad (2)$$

where ω_0 is the resonant frequency, and ω_1 and ω_2 are the frequencies at which the amplitude of oscillation reduces to $1/\sqrt{2}$ of the maximum value. The estimated uncertainties for tan(ϕ) and G' were less than 2% and 5%, respectively.

3. *Results and Discussion*

3.1. *Magnetothermogravimetry*

The temperature dependence of ρ_M(T) shown in Figure 1 reflects the behaviour of the magnetization as a function of temperature for the studied samples (see Table 1).

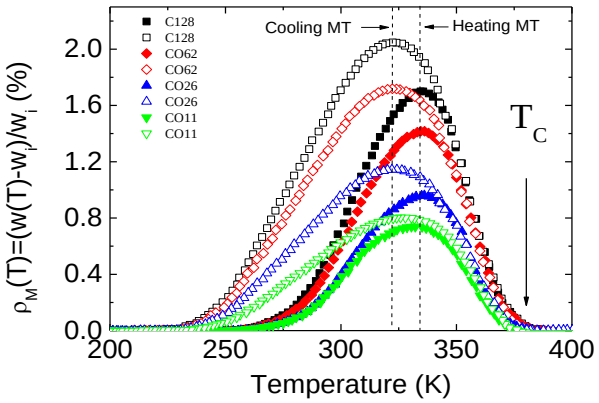

Figure 1: Magnetothermogravimetry (ρ_M(T) = (w(T) – w_i) / w_i) for C011 (inverted triangles), C026 (triangles), C062 (rhombus) and C128 (squares) composite samples. Warming: Full symbols. Cooling: Empty symbols.

During heating, the magnetization first increases when the reverse martensitic transformation takes place (the MSMA fillers transform from a non-magnetic martensite phase to a ferromagnetic austenite phase) and then decreases on approaching the Curie temperature of the austenite (Tc ≈ 380 K) . On the other side, the magnetization increases on cooling below Tc and drastically decreases on further cooling below the forward MT temperature. The structural transformation occurs so close to the magnetic one that the magnetization increase associated to the

ferromagnetic ordering is truncated by the sudden appearance of paramagnetic martensite. This behaviour has been correlated with the weakening of the exchange interactions in the martensitic structure as a consequence of the abrupt change in the Mn-Mn interatomic distances occurring upon the MT [30]. The thermal hysteresis in the MT is around 20 K for the C011 sample, and around 30 K for all the remainder samples. During the MT, the variation of ρ_M(T) increases as the volume fraction of MSMA-fillers increases. The polymer matrix sample (Matrix sample in Table 1) does not show any magnetization change.

3.2. *Dynamic Mechanical Analysis (DMA)*

3.2.1. *Mechanical damping linked to the glass transition*

Figures 2 (a) and (b) show the behavior of tan(ϕ) and G' as a function of temperature for the polymer matrix and for the composites. In the damping spectra, the whole set of composites show a relaxation peak at around 340K linked to the glass transition, Tg, increasing its temperature and decreasing its peak height as the volume fraction of fillers increases. The increases in Tg is promoted by the reduction in the mobility of the polymer chains during the transition due to the embedded fillers [31-34]. In addition, the peak height decreases due to both, the lower fraction of polymer content and the reduced mobility of the polymer chains. As shown in Figure 2 (b), the behavior of the dynamic modulus around the glass transition is similar in all composites. However, the average value of the dynamic modulus increases with the volume fraction of metallic fillers [35-38].

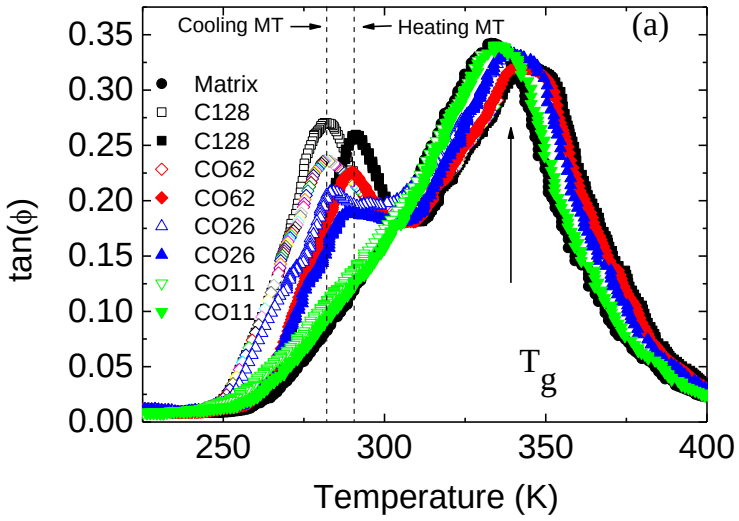
Cooling MT
Heating MT
(a)
Matrix
C128
C128
CO62
CO62
CO26
CO26
CO11
CO11
T_g
tan(ϕ)
Temperature (K)

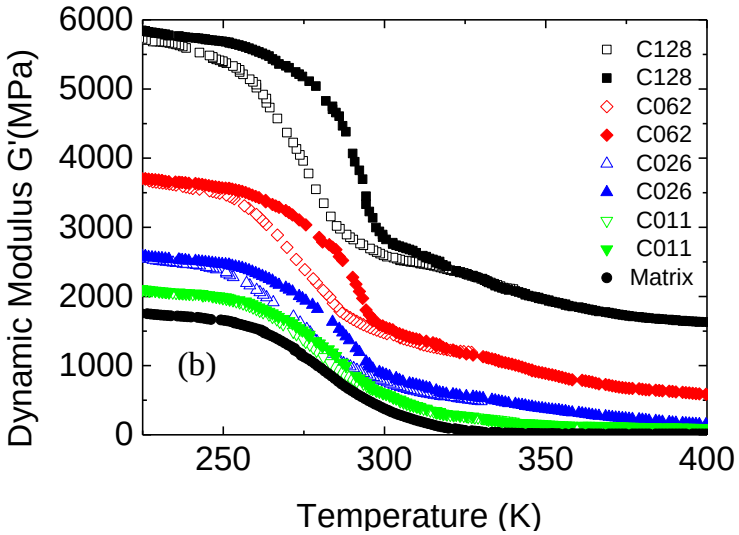
C128
C128
C062
C062
C026
C026
C011
C011
Matrix
(b)
Dynamic Modulus G'(MPa)
Temperature (K)

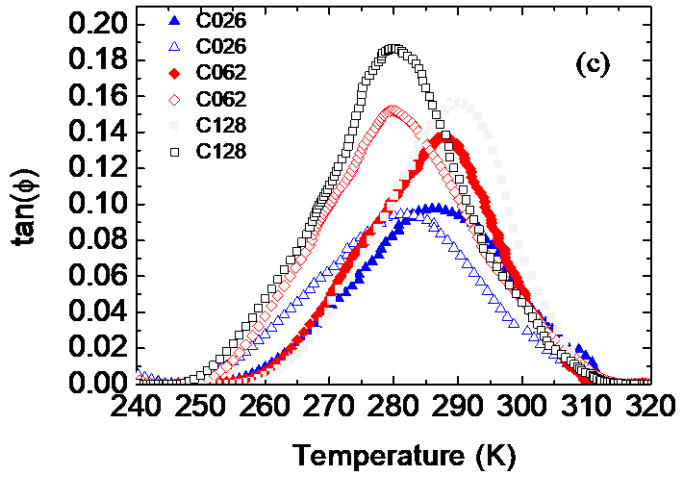

Figure 2: (a): tan(ϕ) spectra. (b): Dynamic modulus curves. (c): Damping spectra after removing the matrix contribution. Matrix sample (circles), C011 sample (inverted triangles), C026 (triangles), C062 sample (rhombuses) and C128 sample (squares). Cooling: Empty symbols, Warming: Full symbols.

3.2.2. *DMA response at the MT without magnetic field*

An hysteresis between cooling and heating measurements is observed below 310 K, both in the damping spectra and in the moduli curves, as shown in Figure 2. This hysteretic behavior is related to the MT taking place between 240 K and 310 K, in agreement with the MTGA measurements shown in Figure 1. Composites with fillers content above 2.6% show a well-defined damping peak at around 285 K (labelled as MT), overlapped on the low temperature side of the glass transition peak. This damping peak in the temperature region where the MT occurs is linked to the high mobility of the austenite-martensite interfaces and to the fact that the temperature, and therefore the transformed fraction, is changing during the measurement cycle, which implies the movement of the transformation front interface [39,40]. Fig. 2(c) shows the damping spectra after removing the matrix contribution. The hysteresis of the MT-peak increases

with the volume fraction of fillers, as shown in Figures 2(a) and (b). Although the MT-peak is not clear in the C011 composite (inverted triangles) due to the low volume fraction of fillers, the hysteresis is observed in both the damping and the shear modulus curves. Once the fillers undergo the phase transformation, i.e. MSMA-fillers are in martensite or in austenite state, the hysteresis vanishes, leading to overlapped cooling and warming curves. The MT-peak height, related to a relaxation process linked to the MT, depends on the warming rate, whereas the peak temperature was frequency independent [39,40]. On the other hand, a dramatic change in the dynamic modulus is observed through the MT, with the modulus of the martensite phase being greater. This behavior can be explained as a consequence of the presence of some soft phonons branches in the austenite (which are indeed responsible for the instability of this phase against distortions such as those linked to MT [41]), implying that some elastic constants, for example $C' = (C_{11} - C_{12})/2$, show very low values. The martensite phase, in turn, does not present these soft modes. The results were reproducible during subsequent thermal cycles. In fact, similar results were obtained in the C128 sample after ten thermal cycles. Thus, it is a promising point in favor of the good mechanical stability of the composites here studied.

3.2.3. *Damping under magnetic field*

Tunable dampers are of especial interest in different applications. In our case, a magnetic field can be used to modify the mechanical response of the bulk composites. In particular, in order to analyze the change of the damping properties, an external magnetic field of 100 kA/m was applied during the DMA measurements.

Figure 3(a) shows the damping spectra for C128 sample measured without (black symbols) and under (red symbols) magnetic field on warming (full symbols) and

on cooling (empty symbols) in the temperature range where the MT takes place (the behavior is similar in all samples, so for sake of clarity just the measurement for the highest concentration composite is shown). In all cases, the maximum temperature reached is 400 K. A slight increase in the MT-peak height (heating and cooling) under magnetic field is observed, in agreement with previous works [42]. Besides, the peak temperature decreases and the hysteresis increases with the applied field, the effect enhancing when the volume fraction of MSMA-fillers increases. As expected, no changes in the damping of the matrix were detected under magnetic field. In the same way, the dynamic modulus curves, Figure 3(b), shift to lower temperatures when measurements are performed under magnetic field.

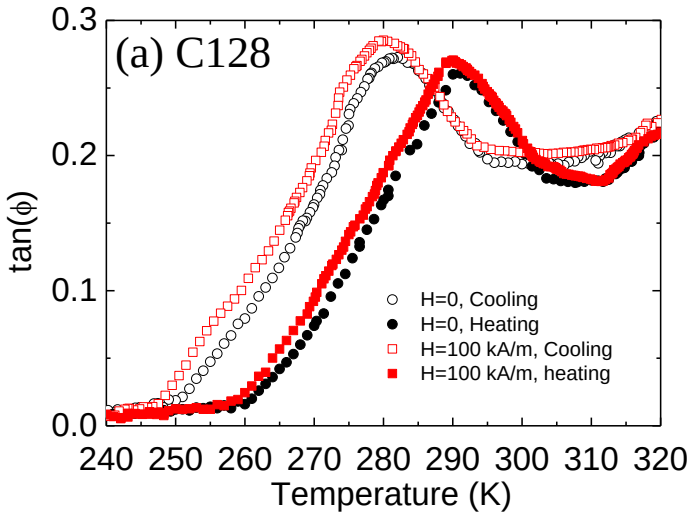

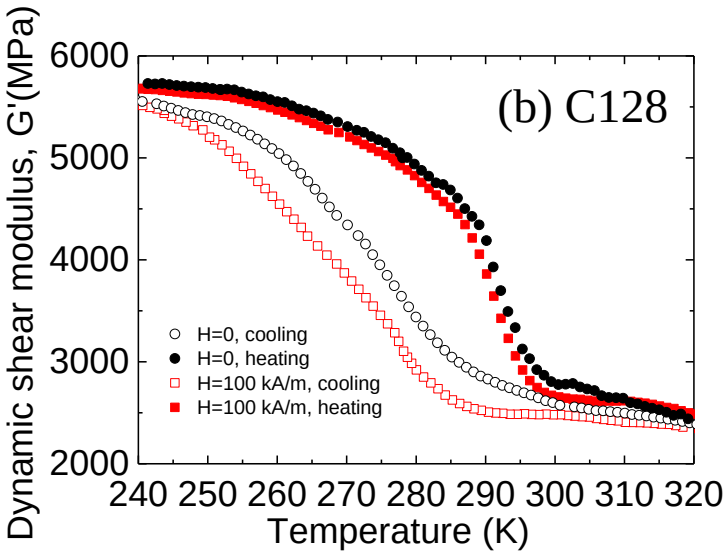

Figure 3: (a) Damping spectra and (b) Dynamic shear modulus for C128 sample with (red symbols) and without (black symbols) external magnetic field, H_{DC} =100 kA/m. Cooling: Empty symbols Warming: full symbols.

Figures 4 (a) and 4 (b) show a summary of the effect of the magnetic field on the hysteresis-width determined from both damping and dynamic modulus (evaluated at the MT-peak temperature) as a function of the volume fraction of fillers.

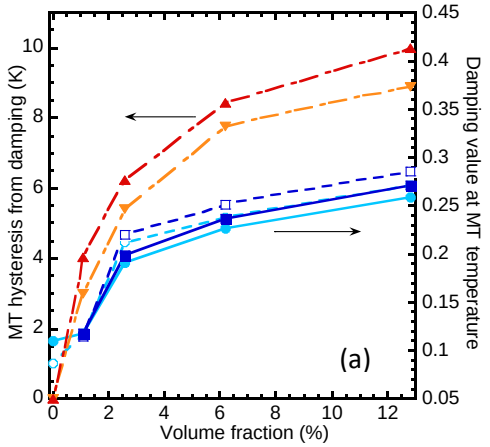

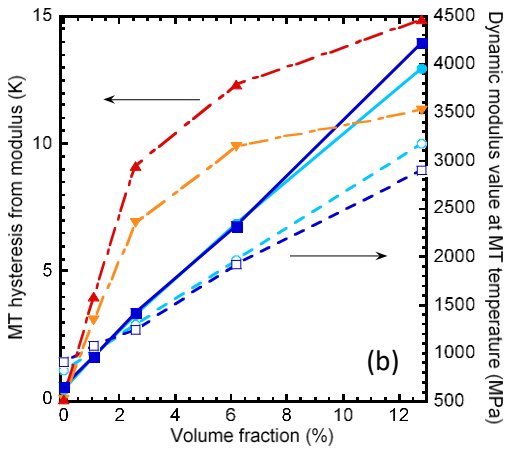

Figure 4: Effect of the magnetic field on the hysteresis-width. (a) Damping as a function of the volume fraction of fillers. Left axis: hysteresis evaluated at the MT-peak temperature; right axis: damping peak height at the MT-peak temperature. (b) Modulus as a function of the volume fraction of fillers. Left axis: temperature hysteresis width from the dynamic modulus evaluated at MT-peak temperature; right axis: Dynamic modulus value at the MT-peak temperature. Direct triangle: hysteresis at H=100 kA/m, inverted triangle: hysteresis at H=0. Light blue circle: heating at H=0, light blue open circle: cooling at H=0, blue square: heating at H=100 kA/m, blue open square: cooling at H=100 kA/m.

As shown in the figure, the application of the magnetic field increases the hysteresis while slightly modifies the damping and the dynamic modulus at the MT temperature. Nevertheless, at lower temperatures the effect of the magnetic field is more evident as shown in figure 3. Therefore, the damping tuning capacity is restricted to the 250-270 K temperature range using these magnetic fields. Higher magnetic fields (not available using the DMA technique) should enhance the effect since the MT shift will be larger. In any case, the figure shows that the higher is the μ-particle volume fraction the higher is the effect of the magnetic field, in agreement with reported results by Nilsén et al. [27] for NiMnGa-epoxy composite material. Magneto-rheological contribution decrease the damping and increase the modulus when the magnetic field increases [34]. Nevertheless, magneto-rheological contribution outside the MT temperature range was not detected in the current composites probably because the low strain amplitude used and the low volume fraction of magnetic fillers present in the composites [27].

In order to understand the increase in the hysteresis, the entropy contributions to the MT must be taken into account. It is well known that a magnetic field induces a shift of the MT temperature according to the Clasius-Clapeyron equation [43]:

$$\frac{dT_{MT}}{dH} = -\mu_0 \frac{\Delta M}{\Delta S} \quad (3)$$

where ΔS, ΔM, T_{MT} , H and μ_0 are the entropy change during the transformation, the difference in magnetization between the austenite and the martensite, the MT-peak temperature, the applied magnetic field and the magnetic permeability in vacuum, respectively. So, a magnetic field shifts the MT towards lower temperatures when the magnetization in the austenite phase is higher than in the martensite phase. In contrast, when the magnetization in the austenite phase is lower than in the martensite phase, the magnetic field shifts the MT temperature towards higher temperatures. The MT of composites undergoes a nearly 2 K shift towards lower temperatures, in agreement with previous works on similar MSMA [44]. As state before, an increase of the MT hysteresis has been observed when the transformation takes place under an applied magnetic field. According to equation (3), the shift of the MT temperature depends on the ratio between ΔS and ΔM. In MSMA, ΔS decreases when the transformation temperature drops due to the counterbalance between the vibrational and magnetic contributions of the MT entropy [45]. On the contrary, ΔM exhibits the opposite behavior, increasing for lower transformation temperatures since the MT takes place from an austenite phase with increasing magnetic order [45]. Thus, the ΔM / ΔS ratio, and therefore the displacement of the transformation temperature with the magnetic field, is greater in the direct transformation (at lower temperatures) than in the inverse one (at higher temperatures). This effect explains the increase of the hysteresis with the magnetic field.

3.2.4. *Evolution of the moduli of MSMA- fillers through the MT*

The change of the elastic and mechanical properties of composites by adding different fillers has been largely analyzed in the literature [32, 35, 46-52]. One of the most used approximation is the Halpin-Tsai model, which allows to calculate the modulus of the fiber-composite with the fibers lying parallel, perpendicular or randomly oriented regarding the applied stress [53]. This model has been also used in rubber-based composites containing carbon nanotubes (CNTs) [54]. In addition, there exist also several works related to the study of the elastic modulus in composite materials as reported in Refs. [55-59]. For instance, Luo et. al., proposed a modification of the Halpin-Tsai model for spherical particles [55] and Li et.al. [59] takes into account the effects of temperature, particles volume fraction, particles radius and the deterioration of the interfacial bonding strength between polymer and fillers. Additionally, Wang et. al. shows an interesting overview about micromechanical models for composites containing nanoparticles [58].

On the other hand, the simplest method to obtain the effective modulus of the composite material is through the rule of mixtures, which could be accepted as a reasonable approximation under small stresses [35]. There are an upper bound given by Voigt model and a lower bound given by Reuss model. The first model supposes that strain is transmitted uniformly trough the material, whereas in the Reuss model it is supposed that the applied external stress is transmitted uniformly trough the material [35].

In the present work, the moduli of the MSMA-fillers around de MT has been determined from the moduli of the composite using a Voigt and Reuss weighted-

average approximation. Equations (4) and (5) represent Voigt (E'_V) and Reuss (E'_R) modulus as a function of temperature.

$$E'_V(T) = fr_i E'_i(T) + fr_m E'_m(T) \quad (4)$$

$$E'_R(T) = \frac{1}{\frac{fr_i}{E'_i(T)} + \frac{fr_m}{E'_m(T)}} \quad (5)$$

where, E'_i, E'_m, fr_i and fr_m are the fillers modulus, the matrix modulus, and the volume fraction of fillers and matrix, respectively.

The actual composite modulus (E') must be in between the Voigt and Reuss bounds. Therefore, our approximation consists in weighting each contribution by means of a p factor ($0 < p \leq 1$):

$$E' = pE'_V + (1-p)E'_R = p\left(fr_i E'_i + fr_m E'_m\right) + (1-p)\frac{1}{\frac{fr_i}{E'_i} + \frac{fr_m}{E'_m}} \quad (6)$$

Then, our mathematical treatment gives rise to a result for E' which would be a bit alike the one obtained from a self-consistent treatment [35]. In the studied composites $E'_i >> E'_m$ and $fr_m > fr_i$, and equation (6) can be transformed to determine the fillers modulus from the experimental data as:

$$E'_i = \frac{E' - p\ fr_m E'_m - (1-p)\frac{E'_m}{fr_m}}{p\ fr_i} \quad (7)$$

The calculus of the effective modulus for the composite material involves the values of the Young moduli for the fillers and the matrix. Nevertheless, in the present calculations we have used the dynamic elastic shear modulus instead of the Young modulus, in agreement with previous works [32,60-62]. Anyway, this will not diminish nor obstruct the subsequent analysis made within a mean field approximation. In

equation (7) the volume fraction of fillers is well known and the RT shear moduli of both, the polymer and the composite can be measured at 300 K. However, the elastic modulus of the MSMA-fillers is also necessary to obtain an adequate "*p*" value. In a previous work, a value of C_{44} = 70 GPa for the cubic austenite at RT has been measured in a Ni-Mn-In-Co single crystal [63]. Then, considering the particles randomly oriented as an isotropic material (C_{44} corresponds to the shear modulus of the fillers) and using equation (7) a value of p = 0.25 is obtained in all composites independently of the volume fraction of fillers.

The temperature dependence of the dynamic modulus of the fillers, with and without magnetic field, calculated for C128 are shown in Figure 5 (the rest of composites overlap the plotted curves and are not shown for clarity); (a) the absolute value and (b) the relative variation with respect to the austenitic state. All curves show a minimum around 280 K related to the direct MT, which has not been clearly detected in the curves in Figure 2(b) and 3(b) since the matrix masks the fillers contribution.

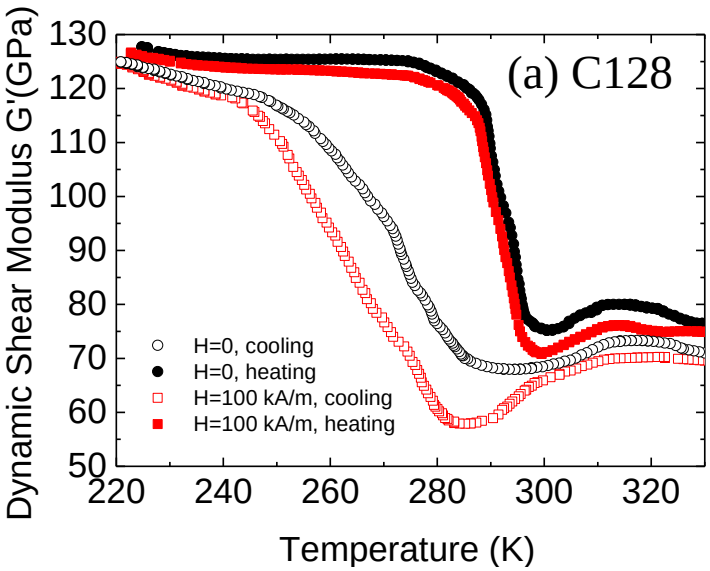

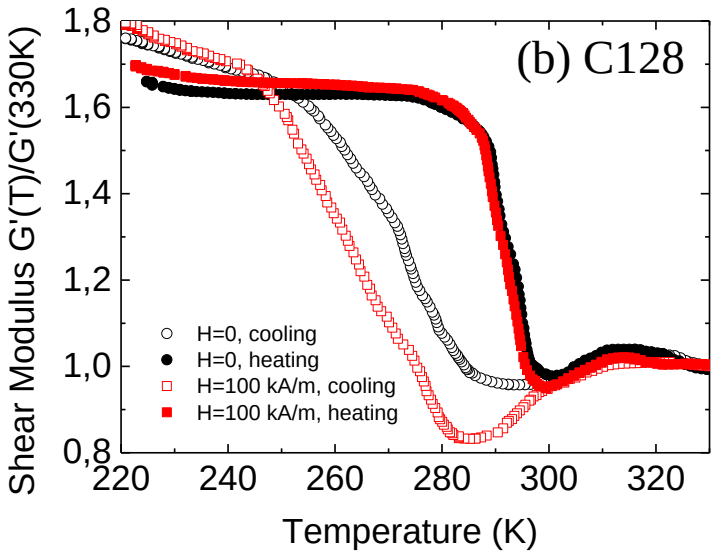

Figure 5: (a) Dynamic shear modulus of the $Ni_{45}Mn_{36.7}In_{13.3}Co_5$ MSMA particles obtained from C128 composite sample using Equation (7) with (red symbols) and without (black symbols) external magnetic field, H_{DC} =100 kA/m. Cooling: Empty symbols Warming: full symbols. (b) Relative variation with respect to the austenite at 330 K.

In addition, the usual hysteresis related to the MT which increases under magnetic field, was also detected in agreement with the above results. It is interesting to note the overlapping of the calculated curves for different volume fraction during the same type of run (heating or cooling) and the same magnetic field condition (with or without magnetic field). In addition, the modulus values in martensitic phase (≈ 125 GPa) are higher than in austenitic phase (≈ 75 GPa) in agreement with the literature for this alloy composition [64,65].

4. *Concluding remarks*

An UV-curing polymer based composite containing $Ni_{45}Mn_{36.7}In_{13.3}Co_5$ MSMA with different percentages of MSMA-particles has been produced for 4D printing

applications. The composites provide a bulk material, containing brittle MSMA- fillers, which can be handled for technological applications. In particular, its damping characteristics have been studied. The composites have a good mechanical stability and reflect the magnetic properties of the fillers. The damping capacity can be tuned when the composites are subjected to an external magnetic field. The metallic fillers slightly shift the glass transition temperature of the polymer to higher temperature. Damping and dynamic modulus of the composites were modified with small magnetic fields below 100kA/m. The degree of tune ability damping properties can be modified by changing the volume fraction of fillers and/or the applied magnetic field. In addition, the mechanical properties of the MSMA particles has been determined from the damping and moduli measurements of the composites with and without applied magnetic field. The intrinsic behavior of the fillers agrees with the well-known bulk counterpart, retaining the characteristic properties linked to the MT. These preliminary results allow proposing this composite material as a potential functional material to be used in the design of printable devices for magneto-mechanical damping applications.

Acknowledgements

This work has been partially supported by PID-UNR ING 575 and ING 612 (2018–2021), Agencia de Investigación de la Provincia de Santa Fe (Cod IO-2017-00138, Res. 177/18), the Project RTI2018-094683-B-C54 (MCIU/AEI/FEDER,UE) and the Cooperation Agreement between the Universidad Pública de Navarra and the Universidad Nacional de Rosario, Res. C.S. 3247/2015.

References

[1] R. Kainuma, Y. Imano, W. Ito, Y. Sutou, H. Morito, S. Okamoto, O. Kitakami, K. Oikawa, A. Fujita, T. Kanomata, K. Ishida, Magnetic-field-induced shape recovery by reverse phase transformation, Nature 439 (2006) 957-960. doi: 10.1038/nature04493.

[2] A. Planes, L. Mañosa, M. Acet, Recent Progress and Future Perspectives in Magnetic and Metamagnetic Shape-Memory Heusler Alloys, Mater. Sci. Forum. 738–739 (2013) 391–399. doi: 10.4028/www.scientific.net/MSF.738-739.391.

[3] J. Liu, T. Gottschall, K.P. Skokov, J.D. Moore, O. Gutfleisch, Giant magnetocaloric effect driven by structural transitions, Nature Mater. 11 (2012) 620–626. doi: 10.1038/nmat3334.

[4] J.I. Pérez-Landazábal, V. Recarte, V. Sánchez-Alarcos, J.J. Beato-López, J.A. Rodríguez-Velamazán, J. Sánchez-Marcos, C. Gómez-Polo, E. Cesari, Giant direct and inverse magnetocaloric effect linked to the same forward martensitic transformation, Sci Rep 7 (2017) 13328. doi: 10.1038/s41598-017-13856-5.

[5] L. Sun, W.M. Huang, Z. Ding, Y. Zhao, C.C. Wang, H. Purnawali, C.Tang, Stimulus-responsive shape memory materials: A review, Mater. & Des. 33 (2012) 577–640. doi: 10.1016/j.matdes.2011.04.065.

[6] J.M. Jani, M. Leary, A. Subic, M.A. Gibson, A review of shape memory alloy research, applications and opportunities, Mater. & Des. 56 (2014) 1078–1113. doi: 10.1016/j.matdes.2013.11.084.

[7] D. Ngo Tuan, A. Kashani, G. Imbalzano, Kate T.Q. Nguyen, D. Hui, Additive manufacturing (3D printing): A review of materials, methods, applications and challenges, Composites Part B 143 (2018) 172-196. doi: 10.1016/j.compositesb.2018.02.012

[8] Z. Chen, Z. Li, L, Junjie, C. Liu, C. Lao, Y. Fu, C. Liu, L. Yang, P. Wang, Y. He, 3D printing of ceramics: A review. J Eur Ceram SOC 39 (2019) 661-667. doi: 10.1016/j.jeurceramsoc.2018.11.013

[9] J. Z. Gul, M. Sajid, M. M. Rehman, G. U. Siddiqui, I. Shah, K-H. Kim, J-W. Lee, K. H. Choi, 3D printing for soft robotics – a review, Science and Technology of Advanced Materials 19 (2018) 243–262. doi: 10.1080/14686996.2018.1431862

[10] Q.Yan, H. Dong, J.Su, J. Han, B. Song, Q. Wei, Y. Shi, A Review of 3D Printing Technology for Medical Applications, Engineering, 4 (2018) 729-742 doi: 10.1016/j.eng.2018.07.021

[11] J. Choi, O-C. Kwon, W. Jo, H.J. Lee, M.-W. Moon, 4D Printing Technology: A Review, 3D Print. Add. Manuf. 2 (2015), 159-167, doi: 10.1089/3dp.2015.0039

[12] X.P. Tan, Y.J. Tan, C.S.L. Chow, S.B. Tor, W.Y. Yeong, Metallic powder-bed based 3D printing of cellular scaffolds for orthopaedic implants: A state-of-the-art review on manufacturing, topological design, mechanical properties and biocompatibility, Mater. Sci. Eng. C 76 (2017) 1328–1343. doi: 10.1016/j.msec.2017.02.094

[13] W. Zhao, F. Zhang, J. Leng, Y. Liu, Personalized 4D printing of bioinspired tracheal scaffold concept based on magnetic stimulated shape memory composites, Comp. Sci. Tech. 184 (2019) 107866. doi: 10.1016/j.compscitech.2019.107866.

[14] B.C. Gross, J.L. Erkal, S.Y. Lockwood, C. Chen, D.M. Spence, Evaluation of 3D Printing and Its Potential Impact on Biotechnology and the Chemical Sciences, Anal. Chem. 86 (2014) 3240–3253. doi: 10.1021/ac403397r

[15] X. Li, R. Cui, L. Sun, K. E. Aifantis, Y. Fan, Q. Feng, F. Cui and F. Watari, 3D-Printed Biopolymers for Tissue Engineering Application, Int. J. Polym. Sci. 2014 (2014) 1–13. doi: 10.1155/2014/829145

[16] C. Barner-Kowollik, M. Bastmeyer, E. Blasco, G. Delaittre, P. Mgller, B. Richter, M. Wegener, 3D Laser Micro- and Nanoprinting: Challenges for Chemistry. Angew. Chem., Int. Ed., 2017, 56, 15828–15845. doi: 10.1002/anie.201704695

[17] J.W. Stansbury and M.J. Idacavage, 3D printing with polymers: Challenges amongexpanding options and opportunities, Dent. Mater. 32 (2016) 54–64. doi: 10.1016/j.dental.2015.09.018

[18] S.C. Ligon, R. Liska, J. Stampfl, M. Gurr, R. Mülhaupt, Polymers for 3D Printing and Customized Additive Manufacturing, Chem. Rev. 117 (2017) 10212–10290. doi: 10.1021/acs.chemrev.7b00074

[19] I.S. Kinstlinger, J.S. Miller, 3D-printed Fluidic Networks as Vasculature for Engineered Tissue, Lab on a Chip 16 (2016) 2025– 2043. doi: 10.1039/C6LC00193A

[20] J.P. Fouassier, J. Lalevée, Photoinitiators for Polymer Synthesis-Scope, Reactivity, and Efficiency, Wiley-VCH Verlag GmbH & Co KGaA, Weinheim, 2012.

[21] N.S. Allen, Photochemistry and photophysics of polymer materials, John Wiley & Sons Inc, New York, 2010.

[22] M. Lahelin, I. Aaltio, O. Heczko, O. Söderberg, Y. Ge, B.Löfgrena, S.-P.Hannulab,J.Seppäläa, DMA testing of Ni–Mn–Ga/polymer composites. Compos. Part A Appl. Sci. Manuf. 40 (2009) 125-129. doi: 10.1016/j.compositesa.2008.10.011.

[23] N. Scheerbaum, D. Hinz, O. Gutfleisch, K.H. Müller, L. Schultz. Textured polymer bonded composites with Ni–Mn–Ga magnetic shape memory particles. Acta Mater. 55 (2007) 2707-2713. doi: 10.1016/j.actamat.2006.12.008.

[24] J. Feuchtwanger, M.L. Richard, Y.J. Tang, A.E. Berkowitz, R.C. O'Handley, S. M. Allen, Large energy absorption in Ni–Mn–Ga/polymer composites, J Appl. Phys. 97 (2005) 10M319. doi: 10.1063/1.1857653.

[25] J. Liu, N. Scheerbaum, S. Kauffmann-Weiss, O. Gutfleisch, NiMn-based alloys and composites for magnetically controlled dampers and actuators. Adv. Eng. Mater. 14 (2012) 653-667. doi: 10.1002/adem.201200038.

[26] B. Tian, F. Chen, Y. Tong, L. Li, Y. Zheng. Magnetic field induced strain and damping behavior of Ni–Mn–Ga particles/epoxy resin composite. J. Alloys Comp. 604 (2014) 137-141. doi: 10.1016/j.jallcom.2014.03.100.

[27] F. Nilsén, I. Aaltio, S.P. Hannula, Comparison of magnetic field controlled damping properties of single crystal Ni-Mn-Ga and Ni-Mn-Ga polymer hybrid composite structures, Comp. Sci. Tech. 160 (2018) 138-144. doi: 10.1016/j.compscitech.2018.03.026.

[28] W. Ito, X. Xu, R.Y. Umetsu, T. Kanomata, K. Ishida, R. Kainuma, Concentration dependence of magnetic moment in $Ni_{50-x}Co_xMn_{50-y}Z_y$ (Z= In, Sn) Heusler alloys, Appl. Phys. Lett. 97 (2010) 242512. doi: 10.1063/1.3525168.

[29] O.A. Lambri, A review on the problem of measuring nonlinear damping and the obtainment of intrinsic damping, in: J. Martinez-Mardones, D. Walgraef C.H. Wörner (Eds.), Materials Instabilities, World Scientific Publishing, New York, 2000, pp. 249-280.

[30] V.V. Khovaylo, T. Kanomata, T. Tanaka, M. Nakashima, Y. Amako, R. Kainuma, R. Y. Umetsu, H. Morito, H. Miki, Magnetic properties of $Ni_{50}Mn_{34.8}In_{15.2}$ probed by Mössbauer spectroscopy, Phys. Rev. B 80 (2009) 144409. doi: 10.1103/PhysRevB.80.144409

[31] I.M. Ward, J. Sweeney. Mechanical properties of solid polymers, John Wiley & Sons, West Sussex, 2012.

[32] R.R. Mocellini, O. A. Lambri, C. L. Matteo, J.A. García, G.I. Zelada-Lambri GI, P.A.Sorichetti, F.Plazaola, A.Rodríguez-Garraza, F.A.Sánchez, Elastic misfit in two-phase polymer, Polymer 50 (2009) 4696-4705. doi: 10.1016/j.polymer.2009.07.037.

[33] O. A. Lambri, D. Gargicevich, F. Tarditti, F. G. Bonifacich, W. Riehemann, M. Anhalt, B. Weidenfeller, Magnetic field dependent damping of magnetic particle filled polypropylene, Solid State Phenom 184 (2012) 449-454. doi: 10.4028/www.scientific.net/SSP.184.449.

[34] R.R. Mocellini, O.A. Lambri, D. Gargicevich, F. G. Bonifacich, B. Weidenfeller, M. Anhalt, W. Riehemann, Magnetic memory effect in magnetite charged polypropylene composite, Composite Interfaces 24 (2017) 611-633. doi: 10.1080/09276440.2017.1250548

[35] T. Mura, Micromechanics of defects in solids. New York: Martinus Nijhoff Publishers; 1987.

[36] O.A. Lambri, J. A. Garcia, W. Riehemann, J. A. Cano, G. I. Zelada-Lambri, F. Plazaola, Dislocation Movement in WE43 Magnesium Alloy during Recovery and Recrystallisation. Mater. Trans. 52 (2011) 1016-1025. doi: 10.2320/matertrans.M2010374.

[37] O.A. Lambri, W. Riehemann, Recovery and recrystallisation processes in plastically deformed WE43 alloy. Int. J. Mater. Res. 102 (2011) 1438-1445. doi: 10.3139/146.110611.

[38] O.A. Lambri, W. Riehemann, Z. Trojanová. Mechanical spectroscopy of commercial AZ91 magnesium alloy. Scr. Mater. 45 (2001) 1365-1371. doi: 10.1016/S1359-6462(01)01171-X.

[39] R. Schaller, G. Fantozzi, G. Gremaud (Eds.), Mechanical Spectroscopy, Trans Tech Publications, Zurich, 2001.

[40] R.B. Pérez-Sáez, V. Recarte, M. L. Nó, J. San Juan, Anelastic contributions and transformed volume fraction during thermoelastic martensitic transformations, Phys. Rev. B 57 (1998) 5684 – 5692. doi: 10.1103/PhysRevB.57.5684

[41] A. Planes, Ll. Mañosa, Vibrational Properties of Shape-Memory Alloys, Solid State Phys. 55 (2001).159–267. doi: 10.1016/S0081-1947(01)80005-9

[42] N. Kartasheva, Y. Liubimova, D. Salas, S. Kustov, Dynamic magnetic characteristics during martensitic transformations in NiMnInCo metamagnetic shape memory alloy, Mater. Today Proc. 4 (2017) 4768-4772. doi: 10.1016/j.matpr.2017.04.068.

[43] A. Planes, Ll. Mañosa, M. Acet, Magnetocaloric effect and its relation to shape-memory properties in ferromagnetic Heusler alloys, J. Phys: Condens. Matter. 21 (2009) 233201. doi: 10.1088/0953-8984/21/23/233201

[44] J.A. Monroe, I. Karaman, B. Basaran, W. Ito, R.Y. Umetsu, R. Kainuma, K. Koyama, Y.I. Chumlyakov, Direct measurement of large reversible magnetic-field-induced strain in Ni–Co–Mn–In metamagnetic shape memory alloys, Acta Mater. 60 (2012) 6883-6891. doi: 10.1016/j.actamat.2012.07.040.

[45] V. Recarte, J.I. Pérez-Landazábal, V. Sánchez-Alarcos, V. Zablotskii, E. Cesari, S. Kustov, Entropy change linked to the martensitic transformation in metamagnetic shape memory alloys, Acta Mater. 60 (2012) 3168–3175. doi: 10.1016/j.actamat.2012.02.022.

[46] J.D. Eshelby, The determination of the elastic field of an ellipsoidal inclusion, and related problems, Proc. R Soc Lon. A. 241 (1957) 376-396. doi: 10.1098/rspa.1957.0133.

[47] T. Mori, K. Wakashima, Successive iteration method in the evaluation of average fields in elastically inhomogeneous materials, in: G.J. Weng, M. Taya, H. Abé (Eds.),

Micromechanics and Inhomogeneity, Springer, New York, 1990, pp. 269-282. doi: 10.1007/978-1-4613-8919-4_18.

[48] M. Kato, T. Fujii, S. Onaka, Elastic strain energies of sphere, plate and needle inclusions, Mater. Sci. Eng. A, 211 (1996) 95-103. doi: 10.1016/0921-5093(95)10091-1.

[49] L. Brison, W.G. Knauss, Finite element analysis of multiphase visco elastic solid. J Appl Mech, 59 (1992) 730-737. doi: 10.1115/1.2894035.

[50] J.K. Lee, Y.Y. Earmme, H.I. Aaronson, K.C. Russell, Plastic relaxation of the transformation strain energy of a misfitting spherical precipitate: ideal plastic behaviour, Metall. Trans. A, 11 (1980) 1837-1847. doi: 10.1007/BF02655099.

[51] T. Mori, K. Tanaka, Average stress in matrix and average elastic energy of materials with misfitting inclusions, Acta Metall. 21 (1973) 571-574. doi: 10.1016/0001-6160(73)90064-3.

[52] Y. Hua, L. Gu, Prediction of the thermomechanical behavior of particle-reinforced metal matrix composites, Comp. Part B, 45 (2013) 1464-1470. doi: 10.1016/j.compositesb.2012.09.056.

[53] J.E. Ashton, J.C. Halpin, P.H. Petit, Primer on Composite Analysis, Chapter 5, Technomic Publishing Co., Stamford, 1969.

[54] A. De Falco, M. Lamanna, S. Goyanes, N.B. D'Accorso, M.L. Fascio, Thermomechanical behavior of SBR reinforced with nanotubes functionalized with polyvinylpyridine, Physica B, 407 (2012) 3175-3177. doi: 10.1016/j.physb.2011.12.057.

[55] Z. Luo, X. Li, J. Shang, H. Zhu, D. Fang, Modified rule of mixtures and Halpin–Tsai model for prediction of tensile strength of micron-sized reinforced composites and

Young's modulus of multiscale reinforced composites for direct extrusion fabrication, Adv. Mech. Eng. 10 (2018) 1687814018785286. doi: 10.1177/1687814018785286.

[56] S.Y. Fu, G. Xu, Y.W. Mai, On the elastic modulus of hybrid particle/short-fiber/polymer composites, Comp. Part B 33 (2002) 291-299. doi: 10.1016/S1359-8368(02)00013-6.

[57] Y. Sliozberg, J. Andzelm, C.B. Hatter, B. Anasori, Y. Gogotsi, A. Hall, Interface binding and mechanical properties of MXene-epoxy nanocomposites, Comp. Sci. Tech. (2020) 108124. doi: 10.1016/j.compscitech.2020.108124.

[58] H.W. Wang, H.W. Zhou, R.D. Peng, L. Mishnaevsky Jr, Nanoreinforced polymer composites: 3D FEM modeling with effective interface concept, Comp. Sci. Tech. 71 (2011) 980-988. doi: 10.1016/j.compscitech.2011.03.003.

[59] Y. Li, W. Li, X. Lin, M. Yang, Z. Zhao, X. Zhang, P. Dong, N. Xu, Q. Sun, Y. Dai, X. Zhang, L. Chen, Theoretical modeling of the temperature dependent tensile strength for particulate-polymer composites, Comp. Sci. Tech. 184 (2019) 107881. doi: 10.1016/j.compscitech.2019.107881.

[60] R.R. Mocellini, G.I. Zelada-Lambri, O.A. Lambri, C.L. Matteo, P.A. Sorichetti, Electrorheological description of liquid and solid dielectrics applied to two-phase polymers: A study of EPDM, IEEE Trans. Dielectr. Electr. Insul. 13 (2006)1358-1370. doi: 10.1109/TDEI.2006.258208.

[61] O.A. Lambri, R.R. Mocellini, F. Tarditti, F.G. Bonifacich, D. Gargicevich, G.I. Zelada-Lambri, C.E. Boschetti, Internal stresses in the electrostriction phenomenon viewed through dynamic mechanical analysis studies conducted under electric field, IEEE Trans. Dielectr. Electr. Insul. 21(2014), 2070-2080. doi: 10.1109/TDEI.2014.004365.

[62] O.A. Lambri, F. Plazaola, E. Axpe, R.R. Mocellini, G.I. Zelada-Lambri, J.A. García, C.L. Matteo, P.A. Sorichetti, Modification of the mesoscopic structure in neutron irradiated EPDM viewed through positron annihilation spectroscopy and dynamic mechanical analysis, Nuclear Inst. Meth. B 269 (2011) 336–344. doi: 10.1016/j.nimb.2010.11.095

[63] J.I. Pérez-Landazábal, V. Recarte, V. Sánchez-Alarcos, M. Jiménez Ruiz, E. Cesari, Outstanding role of the magnetic entropy in arrested austenite in an ordered Ni45Mn36.7In13.3Co5 metamagnetic shape memory alloy, Scripta Mater. 168 (2019) 91–95. doi: 10.1016/j.scriptamat.2019.04.035

[64] D. Salas, E. Cesari, I. Golovin, S. Kustov, Magnetomechanical and structural internal friction in Ni-Mn-In-Co metamagnetic shape memory alloy, Solid State Phenom. 184 (2012) 372-377. doi: 10.4028/www.scientific.net/SSP.184.372.

[65] N. Kartasheva, Y. Liubimova, D. Salas, S. Kustov, Dynamic magnetic characteristics during martensitic transformations in NiMnInCo metamagnetic shape memory alloy, Mater Today Proc. 4 (2017) 4768-4772. doi: 10.1016/j.matpr.2017.04.068.